ELSEVIER

Colloids and Surfaces
A: Physicochemical and Engineering Aspects 190 (2001) 81–88

COLLOIDS AND SURFACES A

www.elsevier.com/locate/colsurfa

Position correlation microscopy: probing single particle dynamics in colloidal suspensions

Stuart Henderson, Steven Mitchell, Paul Bartlett *

School of Chemistry, University of Bristol, Cantock's Close, Bristol BS8 1TS, UK

Abstract

A novel optical tweezer based microscope is described which probes the dynamics of an individual pair of colloidal particles over many decades of time, with nanometer position resolution. The potential of the technique is demonstrated by probing the distance dependence of the hydrodynamic forces between two polymer-coated poly(methyl methacrylate) spheres suspended in cyclohexane.

Keywords: Optical tweezers; Hydrodynamics; Hard-sphere colloids; Brownian motion; Microscopy

1. Introduction

As our ability to control the bulk properties of colloidal systems has improved there has been a rapid growth of interest in understanding the microscopic processes which occur at the *single* particle level within a suspension. Traditional experimental methods such as light, X-ray and neutron scattering generate average values from essentially a very large number of copies of the suspension. Such ensemble measurements integrate the information on the microscopic properties of interest over the whole of thermal phase space. Of course, the results are still of great value but they can only provide indirect insights into the fundamental microscopic process which most interest us. Direct access to the forces and dynamics of individual colloidal particles would allow for a scrutiny of the microscopic processes at high resolution without ensemble averaging.

The task of manipulating and measuring the properties of a single colloidal particle within a suspension is daunting. Electrostatic or entropic colloidal forces on an individual particle are typically of the order of 100 fN while the forces may change substantially on a length scale of a few nanometers. Any attempt to measure single colloid properties requires therefore an instrument with high temporal and force resolution which will function in the presence of significant thermal motion. Various methods have been developed in the past for this task including optical [1,2], magnetic traps [3] and atomic force microscopy [4]. In this paper a novel experimental technique is described which probes *directly* the microscopic forces acting on a pair of colloidal spheres over many decades in time, with a sensitivity of a few tens of femtonewtons and a sub-nanometer posi-

* Corresponding author. Tel.: +44-1225-826118; fax: +44-1225-826231.

E-mail address: p.bartlett@bristol.ac.uk (P. Bartlett).

0927-7757/01/$ - see front matter
PII: S0927-7757(01)00667-7

tion resolution. The position correlation microscope uses a pair of strongly focussed laser beams to trap two colloidal spheres at a defined separation. Thermal fluctuations in the positions of the spheres are measured by imaging the focused laser beams onto a pair of quadrant photodetectors. Forces that act between the two spheres are determined with high resolution by computing the cross correlation between the instantaneous position of each particle. Below we present the physical implementation of this technique and describe a simple experiment which demonstrates that the technique works.

2. Experimental methods

Fig. 1 depicts a schematic diagram of the experimental setup. The position correlation microscope is based around a standard inverted microscope (Axiovert S100, Zeiss) equipped with high numerical aperture optics. A pair of independent optical traps were formed by focussing two orthogonally polarised beams from a Nd:YAG laser (7910-Y4-106, Spectra Physics) with a wavelength of $\lambda = 1064$ nm to diffraction-limited spots in the sample using an oil-immersion microscope objective ($100\times/1.3$ NA Plan Neofluar, Zeiss). The back aperture of the objective lens was overfilled to ensure high trapping efficiency. The power of each laser beam, in the focal plane, was continuously adjustable up to a maximum of about 80 mW. Laser intensities above 2 mW were just sufficient to hold the colloidal particles, used in the current work, within the focus of the beam. The location of each polarised beam and thus the trapped particle [5] was simply controlled by adjusting the associated gimbal mounted mirror (GM) and the 1:1 telescope, formed by the pair of lens L_1 and L_2 detailed in Fig. 1. Altering the positions of these components allowed the mean separation of the two trapped spheres to be varied continuously between 2 and 30 μm. The exact positions of the centres of the two traps were determined to within 40 nm using video microscopy and a centroid tracking algorithm.

While the *mean* position of each particle was fixed by the position of the corresponding laser focus, fluctuating thermal forces caused small but continuous displacements of the particle away

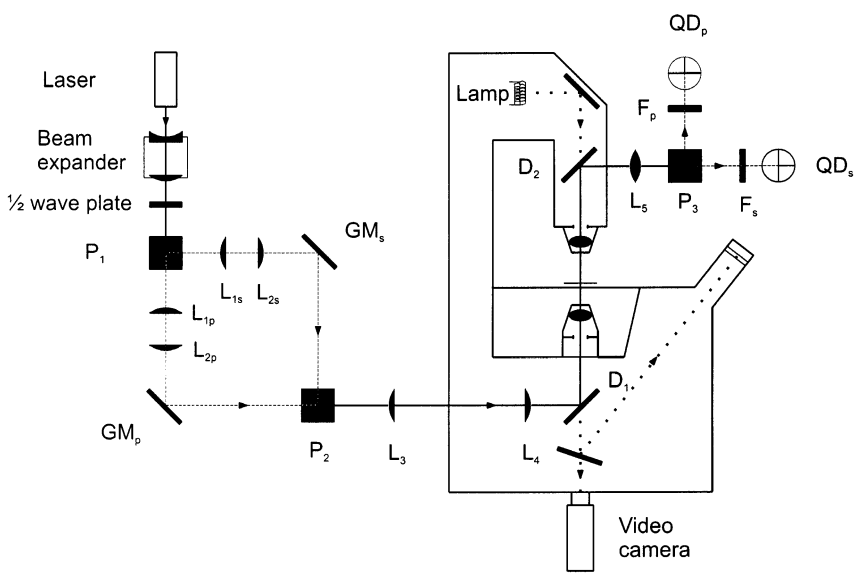

Fig. 1. Schematic diagram of the dual-beam optical tweezer setup. The lens L_{1s} and L_{2s} form a 1:1 telescope for the S-polarised beam which together with the gimbal mounted mirror GM_s are used to adjust the position of the S-polarised beam within the focal plane. The components L_{1p}, L_{1p} and GM_p do the same for the P-polarised beam. P_1, P_2 and P_3 are polarising beam splitting cubes, D_1 and D_2 are dichroic mirrors, F_s and F_p are 1064 nm line filters and QD_s and QD_p are the two quadrant detectors.

from the centre of the trap. For small displacements in the plane of the sample the optical trapping potential is approximately harmonic. The restoring force on the particle is then simply proportional to the lateral displacement, $F = -k_L(x+y)$, with a lateral force constant k_L which for a given particle and beam profile is a linear function of the laser power. In the experiments detailed below the trap spring constants were normally of the order of 10^{-5} N m^{-1}.

Measurements were performed on poly(12-hydroxy stearic acid) stabilised poly(methyl methacrylate) (PMMA) spheres [6] of radius 0.71 ± 0.02 μm dispersed in a layer of cyclohexane 170 μm thick. The volume fraction of particles in the suspension was very low, of the order of 5×10^{-6} to minimise the interference from stray spheres diffusing into the traps during measurements. A small concentration of free stabiliser was added to the suspension to minimise the adsorption of colloidal particles onto the glass walls of the cell. The suspensions were contained in rectangular glass capillaries with a wall thickness of 170 μm which were hermetically sealed with an epoxy resin to prevent evaporation.

On the microseconds timescale characteristic of our experiments, the motion of a colloidal particle is heavily damped by viscous coupling with the fluid. Inertial terms are negligible and the net force on a particle is essentially zero. Any colloidal force on a particle is balanced by an equal and opposite optical restoring force. Consequently the thermal forces on a trapped colloidal particle may be computed from the instantaneous position of the particle. To determine the positions of each of the two trapped spheres with high resolution the interference pattern between the transmitted and scattered laser light was observed in the back-focal plane of the microscope condenser [7]. Motion of a refractive particle in the highly inhomogeneous field at the laser focus significantly changes the amplitude of the forward scattered light. Constructive interference with the transmitted beam occurs in the back-focal plane of the condenser and causes intensity shifts which are imaged by the lens L_5 onto a quadrant detector. The interference signals arising from the two orthogonally polarised beams are separated using a polarising beam-splitter (P_3) and amplified by two custom-built current-to-voltage converters. Difference signals from the sum of the horizontal (X) and vertical (Y) halves of the quadrant detectors and the total signal from each photodiode are calculated by analogue electronics before being digitised at a frequency of 20 kHz and stored for later analysis. The position detectors were calibrated by analysing the thermal fluctuations of a trapped Brownian particle. The high sensitivity of the quadrant diode detector is illustrated in Fig. 2, which shows the X-voltage response generated by scanning an immobilised particle in 10 nm square-wave steps, using a piezoelectric translation stage (P-517 2CL, Physik Instrumente), through the trap centre. As is clear, the noise on the detector signal is at the nanometer level which for a typical trap stiffness of $k_L \sim 10^{-5}$ N m^{-1} equates to an equivalent force sensitivity of ~ 10 fN.

3. Single particle experiments

To calibrate the force measurements the thermally driven position fluctuations of a single *isolated* particle were studied. Probably the simplest measure of the dynamics of a trapped Brownian particle is the mean-squared displacement a particle undergoes in a time interval τ

$$\langle \Delta x^2(\tau) \rangle = \langle [x(t+\tau) - x(t)]^2 \rangle \quad (1)$$

where $x(t)$ is the instantaneous position of the particle after a time t and $\langle \cdots \rangle$ denotes a time-averaged quantity. The mean-squared displacement $\langle \Delta x^2(\tau) \rangle$ as a function of τ is readily calculated from the measured displacement record $x(t)$. It is obvious that for $\tau = 0$ the mean-squared displacement must start at $\langle \Delta x^2(\tau) \rangle = 0$ while in a focussed beam, since the particle is confined to a restricted region of space, the mean-squared displacement will at long times approach a plateau value $\langle \Delta x^2(\tau \to \infty) \rangle$. Fig. 3 shows the time-dependence of $\langle \Delta x^2(\tau) \rangle$ measured in a 52 s period at three different laser intensities for a 0.71 μm particle trapped in a S-polarised beam 20 μm above the wall of the capillary. It is clear that the measured data shows the time-dependence expected with the plateau value $\langle \Delta x^2(\tau \to \infty) \rangle$ in-

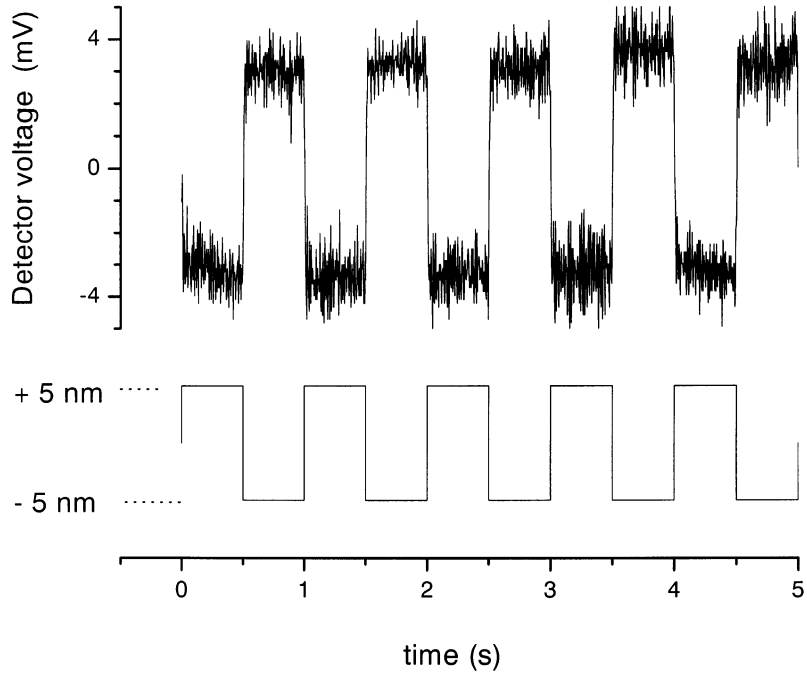

Fig. 2. The top trace shows the X-detector response in millivolts as an immobilised 0.71 μm radius PMMA particle mounted on a piezoelectric stage is driven along the x-axis through the centre of the focussed beam with $a \pm 5$ nm amplitude square wave. The lower trace shows the driving voltage.

creasing with decreasing laser intensity. Interestingly, it is also clear that at short times $\langle \Delta x^2(\tau) \rangle$ decays linearly with a slope that is independent of laser intensity. To quantitatively interpret these observations we assume that the trapping potential is harmonic. The dynamics of a Brownian particle bound in a harmonic potential have been analysed in detail by Uhlenbeck and Ornstein [8]. The problem has two characteristic time scales, τ_f and τ_s, which define the decay time τ_f^{-1} of the velocity autocorrelation function of the Brownian particle and the time τ_s on which the displacement of the Brownian particle is influenced strongly by the potential

$$\tau_f = m/6\pi\eta a \tag{2}$$

$$\tau_s = 6\pi\eta a/k_L$$

Here m is the effective mass of the colloidal particle, η the viscosity, a the particle radius, and k_L the force constant of the harmonic potential. It is instructive to estimate the relevant time scales for the experiments detailed here. For a 0.71 μm radius PMMA particle in cyclohexane, τ_f is about 2×10^{-7} s and all of the current measurements are therefore made in the 'long-time' limit $\tau \gg \tau_f$ where inertial terms are negligible. Secondly, for the harmonic trap stiffnesses used in the current work (typically of order 10^{-5} N m^{-1}) τ_s is of the order of 10^{-3} s. Consequently the fast decay time τ_s is much shorter than the slow decay time τ_s and the dynamics of the Brownian particle are strongly overdamped [9]. In this limit, it is straightforward to demonstrate that for $\tau \gg \tau_f$ the mean-squared displacement is given by the expression

$$\langle \Delta x^2(\tau) \rangle = \langle \Delta x^2(\tau \to \infty) \rangle \times \left[1 - \exp\left\{ -\frac{2D_0\tau}{\langle \Delta x^2(\tau \to \infty) \rangle} \right\} \right] \tag{3}$$

with the free diffusion coefficient, $D_0 = k_B T/6\pi\eta a$ Expansion of Eq. (3) in powers of τ shows that at short times, where $\tau_f < \tau < \tau_s$, the particle diffuses

freely and the mean-squared displacement grows initially linearly with time, $\langle \Delta x^2(\tau) \rangle = 2D_0\tau$. Over longer times the diffusive motion of the particle is gradually retarded by the harmonic potential and the mean-squared displacement eventually saturates at the equilibrium limit $\langle \Delta x^2(\tau \to \infty) \rangle = 2k_B T/k_L$. The solid lines in Fig. 3 show the results of a numerical fit of Eq. (3) to the experimental data with a fixed diffusion constant D_0 calculated from the particle radius and the viscosity at 25°C of cyclohexane ($\eta = 0.894 \times 10^{-3}$ Pa s). It is clear that the harmonic model accounts accurately for the experimental data over some two decades over time and at three different laser intensities.

4. Two particle experiments

A colloidal particle held within an optical trap is subject to continuous, small but measurable fluctuations in position as a result of Brownian forces. As the trapped particle moves a flow is created in the surrounding fluid which causes neighbouring particles to move [10]. Such hydrodynamic coupling is of tremendous importance in

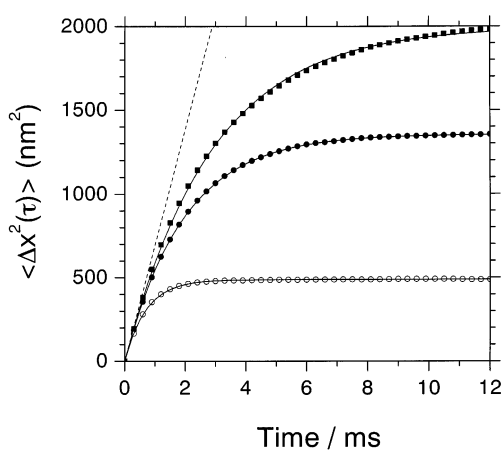

Fig. 3. The time dependence of the mean-squared displacement $\langle \Delta x^2(\tau) \rangle$ of a 0.71 μm PMMA sphere trapped in beams of 13 mW (squares), 18 mW (filled circles), and 43 mW (open circles). 2^{20} data points were collected at a sampling interval of 50 μs. The solid lines are numerical fits using the expression of Eq. (3) and a free diffusion constant $D_0 = 3.46 \times 10^{-13}$ $m^3\,s^{-1}$. The mean-squared displacement of an untrapped sphere is shown dashed.

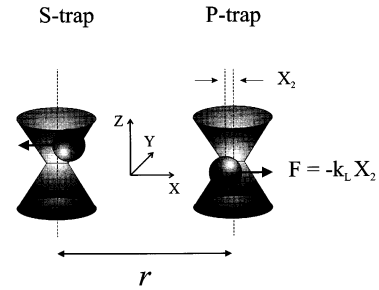

Fig. 4. The geometry of the dual-trap experiments. A pair of spheres is held in the orthgonally polarised S and P traps, spaced a distance r along the x-axis. The arrows show the direction of the optical gradient forces, $F = -k_L x$, when a sphere is displaced a distance x from the centre of the trap.

determining the aggregation, rheology and sedimentation of colloidal suspensions [11]. Yet despite the prevalence and significance of such forces our current theoretical and experimental understanding of hydrodynamic effects in all but the simplest colloidal systems is either sketchy or at best controversial [12]. Theoretical and numerical difficulties stem from the long-range nature of hydrodynamic forces while until recently [1] experimental insights have been limited because conventional techniques such as dynamic light scattering provide only highly averaged rather indirect information on hydrodynamic interactions. Here we describe how optical trapping techniques may be used to measure directly the pair-mobility tensor for two polymer-coated colloidal spheres as a function of the centre-to-centre separation r.

Fig. 4 shows schematically the geometry of our measurements. A pair of polymer-coated PMMA spheres of radius $a = 0.71$ μm, dispersed in cyclohexane, were held in two optical tweezers at a near constant separation r, measured along the x-axis and spaced at least 20 μm from any wall. The separation between the two traps was adjusted between 2.5 and 20 μm. The power in each of the orthogonally polarised beams was carefully adjusted so that the stiffness of the two optical traps were identical. Each beam had a power of typically 30 mW which resulted in a trap stiffness of 9.1×10^{-6} N m^{-1}. Individual spheres move only with a rms amplitude of 21 nm in the trap so

to a good approximation the separation between two trapped spheres is constant and equal to the trap separation r. The location of each sphere, $x_1(t)$ and $x_2(t)$, in the focal plane at the time t was measured with nanometer precision using the calibrated quadrant photodetector system described in Section 2. Similar colloidal systems have been studied by a number of authors [13,14]. These previous studies have established that the interparticle potential is steep, purely repulsive, and well approximated by a hard sphere interaction. Consequently when the two traps are spaced by at least one colloidal diameter ($r > 2a$) no potential interaction between the two spheres is expected. Under such conditions the motions of the two trapped spheres are *not*, however, independent. Thermal fluctuations in the position of each sphere causes the suspending fluid to flow which will influence the position of the second particle. The degree of coupling between the position fluctuations of the two spheres depends on the magnitude of the hydrodynamic forces measured at the fixed trap separation r. Below we detail how the hydrodynamic drag forces may be investigated from a measurement of their effect on the cross-correlation between the position fluctuations of the two trapped spheres.

The dynamics of the two trapped spheres are most readily understood in terms of the normalised cross correlation function $h_{12}(\tau)$ which is defined by the equation

$$h_{12}(\tau) = \frac{(x_1(t+\tau)x_2(t))}{\sqrt{\langle x_1(t)^2\rangle\langle x_2(t)^2\rangle}} \quad (4)$$

where $x_1(t)$ and $x_2(t)$ are the measured x-positions of sphere one and two, respectively, at a time t. h_{12} summarises the statistically averaged correlations between the positions of the two spheres. If, for instance, the motions of the two particles are independent of each other then $h_{12} = 0$ while a positive value signifies that the position fluctuations of the two spheres are, on average, in-phase with a negative value indicating conversely that the position fluctuations are anti-correlated. The asymptotic dependence of $h_{12}(\tau)$ on the delay time τ can be derived from a few straightforward considerations. At long delay times, $\tau \to \infty$, the position of the two spheres will be uncorrelated and $h_{12}(\tau \to \infty)$ will equal zero as the hydrodynamic flows which couples the motion of the two spheres together are dissipative and so must decay to zero at long times. Similarly at short times, $\tau \to 0$, the cross-correlation is also zero as $h_{12}(\tau = 0)$ records only *static* correlations [9] between the particles which, at thermal equilibrium, are a function only of the interparticle potential. In the current experiments there is no potential coupling between the two spheres (at all trap separation $r > 2a$) and so $h_{12}(\tau = 0) = 0$. The cross correlation function is therefore zero at short and long times and non-zero only for intermediate times.

Fig. 5 shows experimental measurements of the cross-correlation functions at three different trap separations r. For a given separation the trapped spheres were followed for a total of 420 s yielding in excess of 8×10^6 samples of their dynamics in intervals of 50 μs. The displacement record was divided into sequences 0.8 s long and the cross correlation function $h_{12}(\tau)$ was computed by a series of fast Fourier transforms. Two features in the experimental data are striking. First, the data shows, rather surprisingly, that hydrodynamic interactions cause the two particles to be *anti-correlated* at intermediate times and second, the degree by which the two particles are anti-correlated increases markedly as the separation between the two particles reduces.

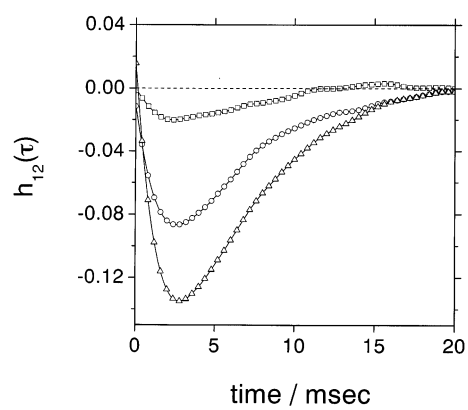

Fig. 5. The normalised cross-correlation h_{12} as a function of delay time τ, measured at three centre-to-centre separations τ. Squares, $r = 15.37$ μm; circles, $r = 4.19$ μm; triangles, $r = 2.50$ μm. Every eighth data point is plotted.

The hydrodynamic forces acting between two spheres in low-Reynolds-number flow have been calculated exactly by a number of authors [15,16]. A key quantity is the mobility matrix μ_{ij} which specifies the instantaneous velocity of particle i when an external force F_j is applied to particle j, through the linear expression $\dot{x}_i = \mu_{ij} F_j$. For a single isolated sphere of radius a in a fluid of viscosity η the mobility coefficient is, from the Stokes equation [10], simply $\mu = 1/6\pi\eta a$. When a second sphere is added, the situation becomes significantly more complicated. The spherical symmetry of the Stokes limit is reduced to axial symmetry and the mobility matrix depends crucially on the geometry of the two spheres [15]. Limiting the present discussion to motion along the line of centres, then it is clear that the off-diagonal element μ_{12} couples the motion of the two spheres together and the coordinates x_1 and x_2 are no longer independent. The motion of the coupled spheres can be decomposed into two independent modes by introducing the normal coordinates

$$X_s = \frac{1}{\sqrt{2}}(x_1 + x_2) \qquad (5)$$

$$X_a = \frac{1}{\sqrt{2}}(x_1 - x_2)$$

which describe in turn a symmetric (X_s) common motion of the centre of mass of the two spheres and an anti-symmetric (X_a) relative motion of the two spheres with respect to each other. The two coordinates X_s and X_a are independent of each other. The corresponding symmetric (μ_s) and anti-symmetric (μ_a) mobilities can be calculated from the asymptotic expressions, valid at large separations, given by Batchelor [15]

$$\mu_s = \frac{1}{6\pi\eta a}\left\{1 + \frac{3}{2\rho} - \frac{1}{\rho^3} - \frac{15}{4\rho^4} + O(\rho^{-6})\right\} \qquad (6)$$

$$\mu_a = \frac{1}{6\pi\eta a}\left\{1 - \frac{3}{2\rho} + \frac{1}{\rho^3} - \frac{15}{4\rho^4} + O(\rho^{-6})\right\}$$

with ρ the dimensionless centre-to-centre separation, $\rho = r/a$. Examination of the lowest order terms shows that the mobility of the symmetric mode is enhanced and the anti-symmetric mode reduced in comparison with an isolated particle. The reduction in mobility of the anti-symmetric mode reflects the increased resistance of the fluid to being squeezed out from the narrow gap between two approaching spheres while the increased mobility for the symmetric mode is caused by the tendency for the fluid flow generated by one sphere to drag along a neighbouring sphere.

The asymmetry in the mobilities of the two normal modes seen in Eq. (6) is reflected in the pronounced anti-correlation observed in the experimental data. The origin of the observed correlation may be understood from a simple physical argument. Thermal fluctuations in the positions of the two spheres may be decomposed into independent fluctuations in the two normal modes. Symmetric fluctuations contribute positively to the cross correlation function h_{12} while the anti-symmetric fluctuations make a negative contribution. At $\tau = 0$ the cross correlation function h_{12} is zero (because there is no potential acting between the two spheres) so the proportion of symmetric and anti-symmetric fluctuations must be equal at $\tau = 0$. In the case where the two spheres are widely separated Eq. (6) demonstrates that the mobilities and hence the decay times for the two modes are identical. Consequently while the contribution of each of the two modes to the cross correlation decays with time their sum remains at zero and $h_{12}(\tau) = 0$ for all times τ. However, when the two spheres are in close proximity to one another the mobility of the symmetric mode is enhanced compared with the anti-symmetric mode. Correspondingly, the decay time for symmetric fluctuations is shorter than the decay time for anti-symmetric fluctuations. As a consequence the cross correlation function develops a pronounced anti-correlation at intermediate times due to the presence of long-lived anti-symmetric fluctuations.

In conclusion, the present study demonstrates that the hydrodynamic coupling between an individual pair of hard-sphere colloids can be accurately measured using a dual-beam optical tweezer. The experimental data shows, rather surprisingly, that the motions of the two particles are anti-correlated at intermediate times. This observation may be understood in terms of the asymmetry of the normal modes for a pair of particles.

Acknowledgements

This work was supported by the Engineering and Physical Sciences Research Council through grant GR/L37533.

References

[1] J.-C. Meiners, S.R. Quake, Phys. Rev. Lett. 82 (1999) 2211.
[2] D. Grier, Curr. Opin. Coll. Interf. Sci. 2 (1997) 264.
[3] O. Mondain-Monval, A. Espert, P. Omarjee, J. Bibette, F. Leal-Calderon, J. Philip, J.-F. Joanny, Phys. Rev. Lett. 80 (1998) 1778.
[4] W.A. Ducker, T.J. Senden, R.M. Pashley, Nature 353 (1991) 239.
[5] E. Fallman, O. Axner, Appl. Opt. 36 (1997) 2107.
[6] L. Antl, J.W. Goodwin, R.D. Hill, R.H. Ottewill, S.M. Owens, S. Papworth, J.A. Waters, Coll. Surfaces 17 (1986) 67.
[7] F. Gittes, C.F. Schmidt, Opt. Lett. 23 (1998) 7.
[8] G.E. Uhlenbeck, L.S. Ornstein, Phys. Rev. 36 (1930) 823.
[9] P.M. Chaikin, T.C. Lubensky, Principles of Condensed Matter Physics, Cambridge University Press, Cambridge, 1995.
[10] J. Happel, H. Brenner, Low Reynolds Number Hydrodynamics, Prentice-Hall, London, 1965.
[11] W.B. Russel, D.A. Saville, W.R. Schowalter, Colloidal Dispersions, Cambridge University Press, Cambridge, 1989.
[12] P.J. Mucha, I. Goldhirsch, S.A. Orszag, M. Vergassola, Phys. Rev. Lett. 83 (1999) 3414. P.N. Segre, E. Herbolzheimer, P.M. Chaikin, Phys. Rev. Lett. 79 (1997) 2574. A.J.C. Ladd, Phys. Rev. Lett. 76 (1996) 1392. D.L. Koch, E.S.G. Shaqfeh, J. Fluid Mech. 224 (1991) 175.
[13] P.N. Pusey, W. van Megen, Nature 320 (1986) 340.
[14] P.N. Pusey, in: J.P. Hansen, D. Levesque, J. Zinn-Justin (Eds.), Liquids, Freezing and Glass Transition, NATO Advanced Study Institute at Les Houches, Session LI, 3–28 July 1989, North Holland, Amsterdam, 1991, pp. 763–942.
[15] G.K. Batchelor, J. Fluid Mech. 74 (1976) 1.
[16] D.J. Jeffrey, Y. Onishi, J. Fluid Mech. 139 (1984) 261.